PCCP

Dynamic Article Links

Cite this: *Phys. Chem. Chem. Phys.*, 2011, **13**, 11412–11421

www.rsc.org/pccp

PAPER

An *in situ* study of the hydriding kinetics of Pd thin films†

Renaud Delmelle and Joris Proost*

Received 3rd December 2010, Accepted 21st April 2011
DOI: 10.1039/c0cp02773a

The hydriding kinetics of Pd thin films has been investigated in detail. The *in situ* experimental technique used in this work consists of a high resolution curvature measurement setup, which continuously monitors the reflections of multiple laser beams reflecting off a cantilevered sample. After mounting the sample inside a vacuum chamber, a H-containing gas mixture is introduced to instantaneously generate a given hydrogen partial pressure (p_{H_2}) inside the chamber. The resulting interaction of hydrogen with the Pd layer then leads to a volume expansion of the thin film system. This induces in turn changes in the sample curvature as a result of internal stresses developing in the Pd film during a hydriding cycle. Based on such *in situ* curvature data, three different kinetic regimes have been resolved. The first two exhibited a linear increase of the internal stress in the compressive direction with time. A systematic study of the p_{H_2}-dependency of the two constant slopes was performed, based on newly derived constitutive kinetic equations. This resulted in the identification of the first linear regime to be limited by absorption and the second one by adsorption. After adsorption equilibrium is reached at the end of the second regime, a third, non-linear kinetic regime, limited by absorption, was found to precede the final hydriding equilibrium. This switch back to absorption-limited kinetics likely occurs due to a coverage dependent change in the adsorption enthalpy of the surface hydrogen. Furthermore, from our *in situ* experimental data, relevant kinetic and thermodynamic hydriding parameters have been derived. As a result, this study was able to provide a self-consistent quantitative interpretation of the entire Pd room temperature hydriding cycle in the alpha-phase domain.

1. Introduction

The interaction of hydrogen with metals has since long been a topic of scientific and technological interest.[1] In particular, the palladium–hydrogen system has attracted intensive research efforts in physical chemistry as a model system because of its high storage capacity, its high sensitivity and selectivity to H_2 gas, and its ability to easily release hydrogen at room temperature.[2] While for hydrogen-storage materials, intermetallic compounds are nowadays considered to be more promising,[3–5] Pd is currently still considered to be a good candidate, especially in thin film form, for applications like hydrogen sensors[6] and gas purification membranes.[7] Additionally, pure Pd is often being used as well in thin film form as a catalytic coating.[8]

Despite the model status of the Pd–H system, the exact kinetic details and the rate-limiting step(s) of room temperature Pd hydriding are still a matter of debate.[6,9] As illustrated schematically in Fig. 1, the Pd hydriding mechanism can be divided into four steps. Firstly, gaseous H_2 molecules need to be adsorbed onto the metallic Pd surface. These adsorbed H_2 molecules then dissociate and the resulting H-atoms slip along a minimum energy path towards atomic well positions, from which they can diffuse into the Pd bulk. A Pd hydride is finally formed, with H-atoms mainly occupying the octahedral interstitial sites of the fcc Pd lattice. Consequently, the composition of the palladium hydride is PdH when all bulk sites are occupied. The configuration of those sites is equivalent

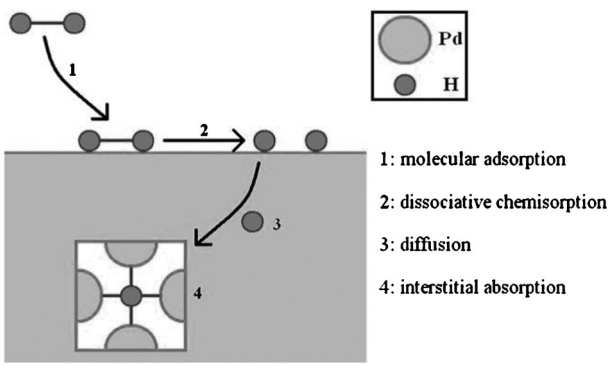

Fig. 1 Schematic representation of the principal kinetic steps involved in Pd hydriding.

Institute of Mechanics, Materials and Civil Engineering, Université catholique de Louvain, Place Sainte-Barbe 2, B-1348 Louvain-la-Neuve, Belgium. E-mail: joris.proost@uclouvain.be; Fax: +32-10-47-40-28; Tel: +32-10-47-93-42

† Electronic supplementary information (ESI) available. See DOI: 10.1039/c0cp02773a

to the positions occupied by strongly chemisorbed H-atoms on a Pd (111) surface.[8] Depending on the amount of absorbed H, expressed as the bulk H/Pd atomic ratio n, there exist, according to the Pd–H phase diagram, two crystalline Pd–H phases, both keeping the fcc structure of the Pd host[1]: α-PdH, with a relatively low hydrogen solubility ($n_{max}(\alpha) = 0.008$ at 298 K) and β-PdH, being a non-stoichiometric hydride with $n_{min}(\beta) = 0.607$ at 298 K. Note that the above-cited room temperature phase stability limits are referring to bulk palladium samples. In the case of Pd nanoparticles, it is now well-established that the miscibility gap becomes narrowed,[10,11] while for thin film samples, the film thickness has been reported to have a significant effect as well on the shape of the pressure–concentration isotherms.[12]

Determining which of those four kinetic steps is rate-limiting is typically based on measuring, preferably *in situ*, the time-evolution of a H-sensitive parameter with respect to p_{H_2}. Such studies have already been reported, based for instance on measurements of Pd cantilever bending,[9] optical reflection or transmission,[6,13,14] dilatometry[15] and resistivity.[16] However, no consensus on an appropriate kinetic model seems to be available yet, neither qualitatively nor quantitatively. For instance, Hu *et al.*[9] claimed a bending rate of their Pd thin film samples depending on $(p_{H_2})^{1/2}$, in agreement with Sievert's law. On the other hand, Zhao *et al.*[6] observed a linear dependence of the hydriding rate with p_{H_2} and therefore concluded that the Pd hydriding mechanism was rather controlled by surface interactions.

In this paper, we report on the use of a high resolution curvature measurement technique to perform more accurate quantitative *in situ* kinetic studies of Pd hydriding than have previously been reported. Although a few other studies have considered curvature monitoring as well,[6,14] none of them have, to the best of our knowledge, been able to reach the same curvature and time resolution as demonstrated in the current paper. This is related to the fact that, unlike current state-of-the-art single-beam curvature measurement techniques, our optical set-up is based on the simultaneous detection of the positions of multiply reflected laser beams into a CCD camera. This has already been shown in a previously published feasibility study to allow for unraveling the kinetics of hydride formation in much more detail.[17] As a result, the presence of different rate-limiting regimes could be recognised for the first time during a single hydriding cycle at constant p_{H_2}. In our previous publication,[17] these were associated, on a rather speculative basis, with the rate of H-absorption and dissociative H-adsorption, respectively.

The current article extends our initial efforts by systematically studying *in situ* the p_{H_2} dependence of Pd hydriding, and analysing the results with newly derived constitutive kinetic equations. This will allow for a full interpretation of the hydriding kinetics, including the identification of different rate-limiting steps. Moreover, its quantitative consistency was confirmed by calculating relevant thermodynamic and kinetic hydriding parameters.

2. Experimental details

Our experimental setup has already been presented in detail in a previous publication.[17] After pumping down a vacuum chamber to base pressures better than 10^{-6} mbar, ultra-pure Ar/H_2 gas mixtures (Alphagaz-grade from Air Liquide) are introduced into the chamber to instantaneously impose a desired total pressure. The latter is continuously measured by two electronic gauges and one back-up manometer. The compositions of the gas mixtures used in this work are 1% and 100 ppm H_2, which allows to further adjust the accessible range of hydrogen partial pressures in the chamber. While hydriding experiments will be reported for p_{H_2} values up to 100 mbar, the quantitative kinetic analysis, which is the main objective of the current paper, has been limited to the low p_{H_2} range (2–10 mbar). As will be shown below, this allows to avoid the α to β hydride phase transition. All experiments have been carried out at room temperature.

A high resolution curvature measurement setup, the optical details of which have already been described earlier as well,[18] is mounted onto the hydriding chamber. It continuously detects the positions of multiple laser beams reflecting off a cantilevered sample, thus allowing to monitor the sample curvature $\Delta\kappa$ in real time:[19]

$$\Delta\kappa = \frac{\cos\alpha}{2L}\frac{\Delta D}{D_0} \quad (1)$$

In eqn (1), $\Delta D/D_0$ is the mean differential spacing between the reflected laser spots in the CCD, L is the distance between the sample and the CCD and α is the angle of laser incidence on the sample. The factor $2L/\cos\alpha$ was calibrated as 1.336 m, based on curvature measurements on mirrors with a known radius of curvature. As compared to other curvature or deflection measurement techniques, which are generally based on the position detection of a single reflecting laser beam, our set-up has a significantly improved dynamic resolution for the radius of curvature on the order of 10 km, thanks to the noise minimization resulting from the concurrent use of multiple laser beams. Moreover, thanks to the use of a CCD camera, curvature measurements can be performed with a time resolution better than 100 ms. The change in internal stress in the Pd layer, which is simply a result of the prohibited volume change during Pd–H interaction in the thin film geometry, can be straightforwardly derived from the measured changes in the sample curvature:[19]

$$\Delta\sigma = \frac{1}{6}\frac{E_S}{1-\nu_S}\frac{t_S^2}{t_f}\Delta\kappa \quad (2)$$

with $E_S/(1-\nu_S)$ the biaxial elastic modulus of the substrate, and t_S and t_f the substrate and Pd film thickness, respectively.

The cantilevered samples used for the kinetic analysis were cut approximately 3×0.5 cm^2 in size from oxidized, 425 μm thick Si wafers. These were coated by e-gun evaporation with a Pd thin film, on top of a 5 nm Ti adhesion layer. The purity and thickness of the Pd films were characterized by ICP/OES measurements on layers dissolved in an acid mixture. No contaminant was detected in concentrations exceeding 10 ppb. The Pd thin film thickness, averaged over ten samples from the same wafer, was found to be 128 ± 1 nm. Our Pd thin films were also shown by X-ray diffraction to exhibit a pronounced (111) texture, typical for vacuum deposited fcc metallic thin films.[20–22] Cu Kα radiation was used and the diffractograms were recorded with an angle step of 0.02°. No secondary (200)

peak was detected. The texture factor was then calculated using the third peak in terms of standard intensity, resulting in $(I_{(111)}/I_{(311)})_{film}*(I_{(311)}/I_{(111)})_{stand} = 38$, where the standard intensity ratio $(I_{(111)}/I_{(311)})_{stand}$ was taken from ref. 23. The initial growth stress in the as-deposited Pd films, which determines the initial baseline stress level for the hydriding cycle, has been determined as well by recording the sample curvature before and after dissolving the Pd layer from the substrate. Such *ex situ* measurements resulted in an average initial tensile growth stress value of 435 ± 3 MPa. Finally, plane-view SEM observations revealed an average grain size of 18 nm. A second batch of Pd films have been deposited under the same conditions in order to perform the experiments that will be reported in Section 3.2 to study the hydriding equilibrium. These films had an average thickness of 112 ± 1 nm, an average grain size of 20 nm, a texture factor of 37 and an average initial tensile growth stress of 409 ± 2 MPa, very similar to the films from the other Pd batch.

3. Results and discussions

3.1 Hydriding cycle

Fig. 2 shows a typical hydriding cycle performed at $p_{H_2} = 6$ mbar. After an initial baseline curvature measurement in high vacuum, the Ar/H_2 gas mixture was instantaneously introduced in the chamber. As a result of the constrained volume expansion during Pd–H interaction, the internal stress in the Pd thin film increases rapidly in the compressive direction and gradually reaches a constant value. The gas mixture was then pumped out of the chamber, resulting in a gradual decrease in the internal stress as a result of room temperature dehydriding.

As to the latter, it appears that the internal stress does not go back to its initial value when the gas mixture is pumped out of the vacuum chamber. In other words, a residual hydriding-induced stress is systematically observed when leaving the sample under vacuum after hydriding. In a previous study performed on the same batch of samples,[17] a multiple cycling experiment was studied in order to get more insight in this phenomenon. It was shown that this residual stress remains constant from cycle to cycle, even if p_{H_2} is changed from one cycle to another. However, the origin of the irreversible part of hydriding under vacuum was not discussed at that stage. An additional single hydriding cycle at $p_{H_2} = 5.5$ mbar is therefore presented in the inset of Fig. 2, including venting with ambient air after dehydriding in vacuum. It is clearly seen that the residual stress is fully released when the sample is brought into contact with ambient air. This observation indicates that the residual stress observed after dehydriding in vacuum can be attributed to a small residual H-concentration in the Pd lattice, the removal of which can be achieved by venting with air so that a fully reversible hydriding cycle is finally obtained.

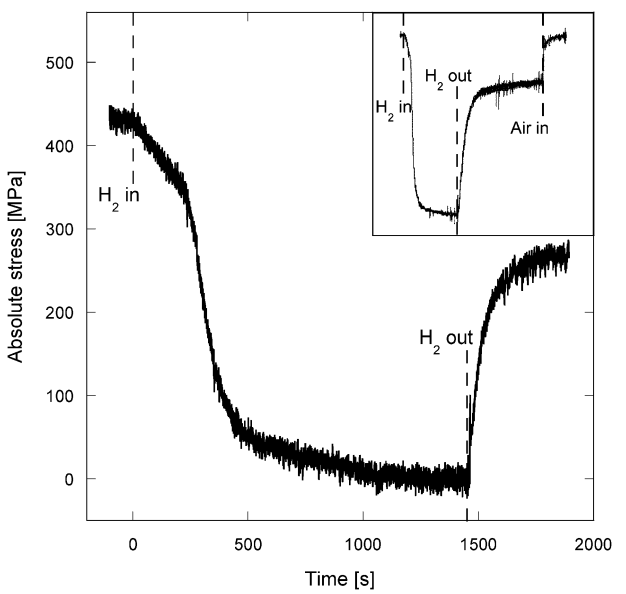

Fig. 2 Evolution of the absolute internal stress as a function of time during a hydriding cycle recorded at $p_{H_2} = 6$ mbar. Inset: hydriding cycle recorded at $p_{H_2} = 5.5$ mbar, including venting with air after dehydriding in vacuum.

From Fig. 2, two distinct kinetic regimes can be distinguished from the two apparently linear regions of the stress–time curve at the beginning of the hydriding cycle. We believe these two slopes to reveal the presence of different rate-limiting steps in the course of a single hydriding cycle. A third regime is resolved in Fig. 2 as well, characterized by a gradual decrease of the hydriding rate with time until a constant equilibrium stress level is reached. The latter can be associated with chemical equilibrium between atomic H inside the Pd thin film sample and gaseous H_2 available in the chamber. Such a characteristic hydriding behaviour with three distinct kinetic regimes has been observed over the entire p_{H_2} interval considered in this paper, and will now be analysed in more detail.

3.2 Hydriding equilibrium

Fig. 3 shows the absolute stress levels corresponding to the equilibrium plateau during hydriding experiments up

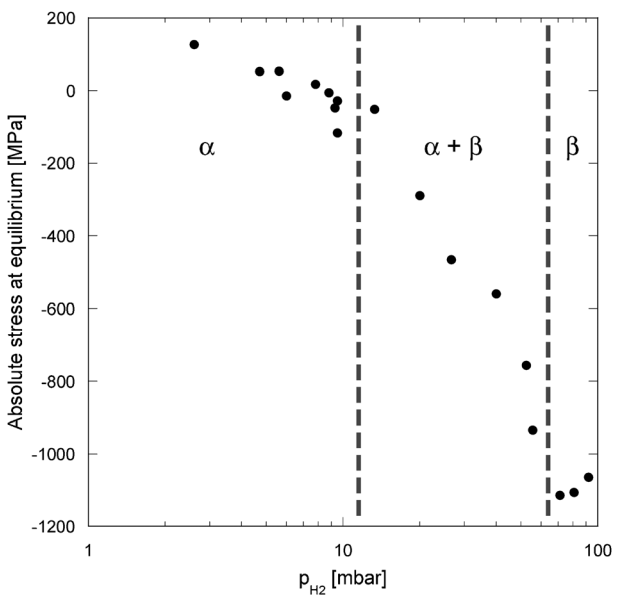

Fig. 3 Equilibrium absolute stress as a function of p_{H_2}. The average initial tensile growth stress in the as-deposited films was 409 ± 2 MPa.

to p_{H_2} = 92 mbar. From these results, the α → β phase transition of Pd-hydride can be identified to start at room temperature between 10 and 20 mbar, in agreement with earlier equilibrium hydriding studies on Pd thin films.[14] As a result, the equilibrium stress levels reached in the p_{H_2}-range that will be considered in the present kinetic study (2–10 mbar) correspond to hydrogen concentrations located in the α phase region of the Pd–H system.

For a quantitative kinetic analysis, a link between the bulk H/Pd atomic ratio n and the measured internal compressive stress change $\Delta\sigma$ in our Pd thin films needs to be established. This can be done by linking $\Delta\sigma$ to the relative volume change $\Delta V/V$ during hydriding:[24]

$$\Delta\sigma = \frac{E_f}{3(1-\nu_f)}\left(\frac{\Delta V}{V}\right) = \frac{E_f}{3(1-\nu_f)}\left(\frac{\Delta v}{\Omega_{Pd}}\right)n \equiv Qn \qquad (3)$$

where E_f and ν_f are, respectively, the Young modulus and Poisson ratio of the Pd film. The ratio between $\Delta V/V$ and n is equal to $\Delta v/\Omega_{Pd}$, where Δv is the characteristic volume change per hydrogen atom, and Ω_{Pd} is the mean atomic volume of a palladium atom. This ratio, describing the lattice expansion due to hydrogen uptake, has been the object of many studies in the past, from which a value of 0.19 ± 0.01 can be derived.[25] Eqn (3) then enables to link the measured hydriding-induced internal stress changes $\Delta\sigma$ to the bulk H/Pd atomic ratio n *via* some mechano-physical constants, which for convenience are grouped together into a single proportionality factor Q.

It should be noted that a possible complicating factor in eqn (3) is the occurrence of an α to β phase transformation during Pd hydriding, each having their own characteristic lattice expansion behaviour so that the measured stress change will depend on the exact proportions of the α and β phases. Although the value of 0.19 has been suggested by Peisl for the whole compositional range in the Pd–H system, the collected data are too scarce to state that there is no effect of the α to β phase transformation on the lattice expansion. However, as already indicated with Fig. 3, this complicating factor does not need to be dealt with in the present study because the α to β phase transformation is avoided by limiting the p_{H_2}-range.

Eqn (3) also makes the explicit assumption that the deformation resulting from the hydriding-induced internal stress is elastic.[26] Thanks to the relatively high initial tensile growth stress of our as-deposited Pd films, and the fact that the kinetic studies have been limited to the α phase region, this condition has been verified as well. In Fig. 2 for instance, it is seen that the equilibrium compressive stress change of this cycle is about 435 MPa. Taking into account the initial tensile growth stress level of 435 MPa in the as-deposited Pd film, this leads to an almost zero equilibrium stress value. Similarly, Fig. 3 shows that, over the entire α phase region, the maximum absolute value of the equilibrium stress level is smaller than 200 MPa, therefore well below the Pd theoretical yield stress.[27] Plastic deformation of our Pd thin films during hydriding in the α phase region can therefore be reasonably excluded. As a result, the time derivative of the hydriding curves obtained experimentally can be considered as directly proportional to the hydriding velocity dn/dt. We can point out as well that these observations also confirm our earlier finding that the residual stress observed in Fig. 2 after dehydriding in vacuum can be attributed to a small residual H-concentration in the Pd lattice.

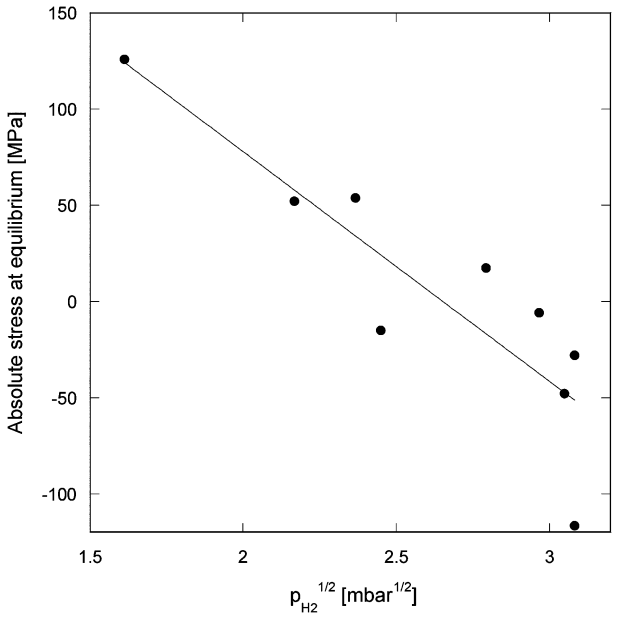

Fig. 4 Equilibrium absolute stress as a function of $(p_{H_2})^{1/2}$ in the α phase region.

Based on the above considerations, we can already use eqn (3) to determine Sievert's constant K_s from our experimentally determined equilibrium stress data in the α phase region of Fig. 3. Indeed, when linearising these data as a function of $(p_{H_2})^{1/2}$, according to Sievert's law in α-PdH:[1]

$$(\Delta\sigma)_{eq} = Qn_{eq} = Q\frac{\sqrt{p_{H_2}}}{K_s} \qquad (4)$$

with n_{eq} the equilibrium atomic hydrogen concentration in the bulk. The slope of the linear fit shown in Fig. 4 yields a K_s value of 3.3 ± 0.7 atm$^{1/2}$ (using E_{Pd} = 121 GPa and ν_{Pd} = 0.39).[28] Room temperature K_s values for Pd hydriding have been reported in a rigorous study by Bucur[29] to be in the range 2–20 atm$^{1/2}$, the higher value corresponding to a perfect crystal structure (*i.e.* well-annealed bulk palladium samples) and the lower one corresponding to a relatively large concentration of structural defects, typical for as-evaporated thin Pd films.[29] Our own value is therefore in excellent agreement with the data from Bucur, recognising that our evaporated Pd thin films probably contain a large defect concentration as well resulting from the deposition process.

3.3 Hydriding kinetics

(a) Constitutive equations. Following our previously reported hydriding study at fixed p_{H_2},[17] we will consider the possibility of 2 mechanistic steps to be rate-limiting during Pd thin film hydriding. One of these steps includes H_2 adsorption and its dissociative chemisorption on the Pd thin film surface, and will conveniently be called adsorption. The other one, denoted as

absorption, is seen as an equilibrium reaction between atomic hydrogen at, respectively, the surface sites and the interstitial sites of the Pd hydride. In his classical hydriding model, Wagner wrote down the following reactions to describe each of these steps:[1]

$$H_2 + 2s \Leftrightarrow 2H\text{-}s \quad (5)$$

$$H\text{-}s + i \Leftrightarrow H\text{-}i + s \quad (6)$$

where s and i are a free surface adsorption site and an interstitial bulk absorption site, respectively, while H-s and H-i represent, respectively, a surface and bulk site occupied by atomic H.

More rigorously, earlier studies claimed the existence of two possible adsorption sites on the Pd (111) surface:[1] the so-called strong and weak adsorption sites, which correspond to, respectively, very deep and rather flat potential wells. The strong adsorption sites are octahedral sites, also called fcc sites.[8] Despite the existence of three other highly exothermic surface sites (called bridge, top and hcp sites), it has been claimed that only the fcc sites need to be taken into account for strong chemisorption on (111) planes of Pd. As indeed suggested by Bucur in one of his thin film hydriding models,[30] the strong adsorption sites are filled well before and much faster than the weak ones.

More recently, Johansson *et al*. obtained accurate computational data for the heat of adsorption on Pd (111) surfaces.[31] The heat of adsorption starts from about -100 kJ mol^{-1} H_2 at zero surface coverage θ, θ being the number of adsorbed hydrogen atoms divided by the number of adsorbed hydrogen atoms in a filled monolayer. It then gradually becomes less negative as θ increases, and rather abruptly takes on positive values somewhere in the range $0.75 < \theta < 1$. This result clearly suggests a more complex adsorption behavior than the one proposed by Bucur. Hong and Rahman arrived at a similar conclusion in their first-principles electronic structure calculations,[32] showing that it is only after a substantial amount of hydrogen is adsorbed on the Pd (111) surface that hydrogen is able to further absorb into the bulk. Similarly, the potential energy surface for hydrogen adsorption/absorption[33] also indicates that a surface that is already substantially covered with hydrogen helps the hydrogen atoms to overcome the energy barrier to move into the bulk.

With respect to the schematics of Fig. 1, no hydrogen diffusion step will be taken into account in the present kinetic model, simply because of the Pd thin film geometry considered in our work. Indeed, one gets a first-order diffusion time on the order of milliseconds when dividing the square of the Pd film thickness by the diffusion coefficient of H-atoms in α-PdH ($D_\alpha \cong 10^{-7}$ cm^2 s^{-1}).[6] This is five orders of magnitude below the time scale of the hydriding kinetics experimentally observed in Fig. 2 for our Pd thin films.

As to the adsorption step, described by reaction (5), an adsorption equilibrium constant K_{ad} can be defined as follows:

$$K_{ad} \equiv \frac{k'_{ad}}{k''_{ad}} = \frac{[H-s]^2_{eq}}{p_{H_2}[s]^2_{eq}} = \frac{\theta^2_{eq}}{(1-\theta_{eq})^2}\frac{1}{p_{H_2}} \quad (7)$$

where θ_{eq} is the equilibrium surface coverage. From reaction (5), the adsorption velocity r_{ad} then takes on the following form:[34]

$$\begin{aligned} r_{ad} &= k'_{ad}(1-\theta)^2 p_{H_2} - k''_{ad}\theta^2 \\ &= k'_{ad}\left[(1-\theta)^2 p_{H_2} - \frac{\theta^2}{K_{ad}}\right] \end{aligned} \quad (8)$$

In a similar way, the absorption equilibrium constant K_{ab} can be deduced from reaction (6):

$$K_{ab} \equiv \frac{k'_{ab}}{k''_{ab}} = \frac{[H-i]_{eq}[s]_{eq}}{[H-s]_{eq}[i]_{eq}} = \frac{1-\theta_{eq}}{\theta_{eq}}\frac{n_{eq}}{1-n_{eq}} \quad (9)$$

Note that the equilibrium constants K_{ad} and K_{ab} can be linked together with Sievert's constant by grouping eqn (4), (7) and (9), and by assuming that $n_{eq} \ll 1$ in α-PdH:

$$K_{ad}K^2_{ab} = \frac{1}{K^2_S} \quad (10)$$

From reaction (6), the absorption velocity r_{ab} can then be written as:

$$\begin{aligned} r_{ab} &= k'_{ab}(1-n)\theta - k''_{ab}n(1-\theta) \\ &= k'_{ab}\left[(1-n)\theta - \frac{n(1-\theta)}{K_{ab}}\right] \end{aligned} \quad (11)$$

Finally, the evolution of the surface coverage θ and bulk H/Pd atomic ratio n can then be deduced by combining the expressions (8) and (11) for the ad- and absorption velocities:

$$\frac{d\theta}{dt} = 2r_{ad} - r_{ab} \quad (12)$$

$$\frac{dn}{dt} = r_{ab} \quad (13)$$

When dealing with complex second order reactions as is the case here, the derivation of general rate expressions taking into account each of the two reaction steps is exceedingly tedious or even impossible to derive. The common alternative method in chemical kinetics then consists in assuming a specific rate-controlling step right from the beginning, and considering the other reaction step to be in a pseudo steady-state.[35] In our case, if we assume that the two constant slopes observed in Fig. 2 during the first and second kinetic regimes reveal the presence of two different rate-limiting steps, we can then derive simplified expressions for the adsorption and absorption velocities by assuming that, respectively, the absorption or adsorption step is in a pseudo steady-state.

Let us first assume that adsorption is the rate-limiting step. In that case, we can consider $k'_{ab} \to \infty$, and as r_{ab} must remain finite according to eqn (11),[35] this leads to $(1-n)\theta - n(1-\theta)/K_{ab} \to 0$, that is to say:

$$\theta = \frac{1}{1 + K_{ab}\frac{1-n}{n}} \cong \frac{n}{n + K_{ab}} \quad (14)$$

This equation then enables to eliminate the unobservable variable θ, since in our experimental approach based on assessing hydriding-induced volume changes, we are only able to access the bulk H/Pd atomic ratio n and not the surface

coverage θ (*cf.* eqn (3)). Inserting eqn (14) into eqn (8) finally gives:

$$r_{ad} = k'_{ad}\left[p_{H_2}\left(\frac{K_{ab}}{K_{ab}+n}\right)^2 - \frac{1}{K_{ad}}\left(\frac{n}{K_{ab}+n}\right)^2\right] \qquad (15)$$

On the other hand, if it is assumed that absorption is the rate-limiting step, one can write $k'_{ad} \to \infty$ so that from eqn (8), similarly as in the reasoning above, $p_{H_2}(1-\theta)^2 - \theta^2/K_{ad} \to 0$. This equation then leads to the following solution for the pseudo steady-state surface coverage θ:

$$\theta = \frac{\sqrt{p_{H_2}K_{ad}}}{1+\sqrt{p_{H_2}K_{ad}}} \qquad (16)$$

Inserting eqn (16) into eqn (11) finally gives:

$$r_{ab} = k'_{ab}\left[\frac{K_{ab}(1-n)\sqrt{p_{H_2}K_{ad}} - n}{K_{ab}\left(1+\sqrt{p_{H_2}K_{ad}}\right)}\right] \qquad (17)$$

Note that eqn (15) and (17), predicting the p_{H_2}-dependences of the adsorption and absorption velocities, have been derived while explicitly assuming $n \ll 1$. This is indeed the case for the range of p_{H_2}-values considered in the present work for room temperature hydriding in the alpha phase region ($n_{max}(\alpha) = 0.008$ in bulk Pd).

(b) Kinetic analysis. After recognising the existence of 2 possible rate-controlling reaction steps, one can reasonably assume, as a starting point for a rigorous kinetic analysis, that the two constant slopes that are systematically observed in the beginning of our hydriding cycles (*cf.* Fig. 2) would correspond to a different kinetic regime, with either ad- or absorption being the rate-limiting step. Since at the beginning of the experiment (when $\theta = 0$ and $n = 0$) the adsorption velocity has already a finite value (*cf.* eqn (8)) while the absorption velocity is still 0 (*cf.* eqn (11)), and since adsorption can be considered as relatively unconstrained on a freshly exposed surface, one could reasonably imagine that the first linear kinetic regime corresponds to an absorption-limited step. The second slope would then be indicative for adsorption to become rate-controlling further on in the hydriding cycle. In order to confirm this assumption, a systematic study of the p_{H_2}-dependence of the measured constant slopes was first carried out.

According to eqn (3), these slopes can be taken proportional to $(dn/dt)_{ab}$ and $(dn/dt)_{ad}$ in each of the 2 "linear" kinetic regimes, respectively. Constitutive equations for these quantities therefore still need to be derived first. As to $(dn/dt)_{ab} \equiv r_{ab}$ (*cf.* eqn (13)), eqn (17) can be further simplified with the additional assumption that $p_{H_2}K_{ad} \gg 1$. At this stage, the latter can be justified from eqn (7), since, from the state-of-the-art discussion in Section 3.3.(a), the equilibrium surface coverage can be considered to be close to one. We will be able to explicitly verify this assumption later in this work, based on derived values for K_{ad}. Combining eqn (17) with eqn (10) and (13) then gives

$$\left(\frac{dn}{dt}\right)_{ab} = k'_{ab}\left[(1-n) - \frac{K_S n}{\sqrt{p_{H_2}}}\right] \qquad (18)$$

An absorption-limited hydriding mechanism can therefore be expected to exhibit a hydriding velocity proportional to $(p_{H_2})^{-1/2}$.

The slope $(dn/dt)_{ad}$ of the second linear regime can be derived by linking the differentials of the surface coverage θ and bulk H/Pd atomic ratio n thanks to eqn (14), resulting in $d\theta = (K_{ab}/(K_{ab}+n)^2)dn$. Combining eqn (15) with eqn (10), (12) and (13) then provides

$$\left(\frac{dn}{dt}\right)_{ad} = \frac{2k'_{ad}K_{ab}^2}{(K_{ab}+n)^2 + K_{ab}}\left[p_{H_2} - (K_S n)^2\right] \qquad (19)$$

indicating that an adsorption-limited hydriding mechanism exhibits a hydriding velocity which can be expected to increase linearly with p_{H_2}.

In Fig. 5, the slopes of the first linear kinetic regime have been plotted as a function of $1/(p_{H_2})^{1/2}$, following constitutive

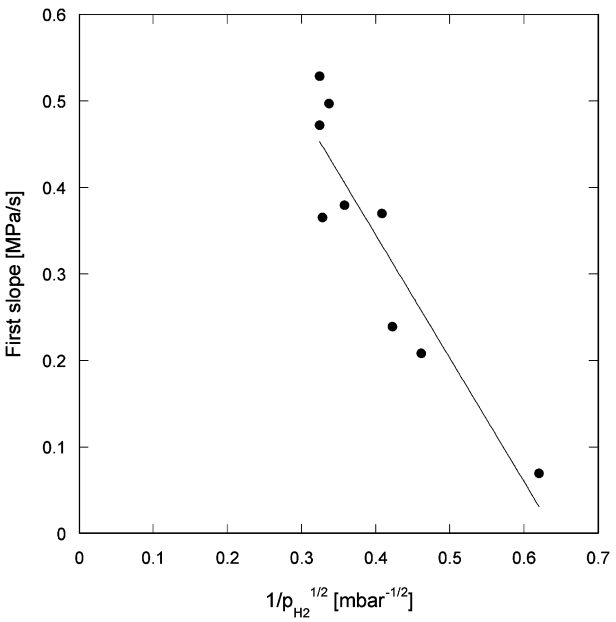

Fig. 5 Slope of the first linear kinetic regime as a function of $1/(p_{H_2})^{1/2}$.

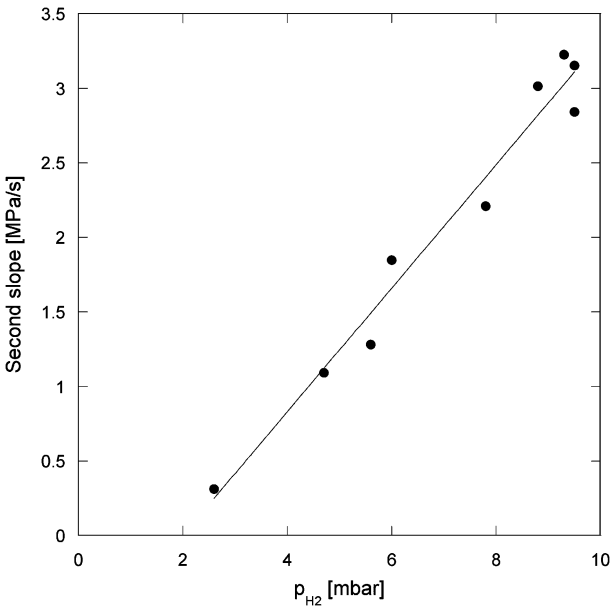

Fig. 6 Slope of the second linear kinetic regime as a function of p_{H_2}.

eqn (18) for an absorption-limited hydriding velocity. Similarly, Fig. 6 shows the slopes of the second linear regime, which exhibit a linear relationship with p_{H_2}, in agreement with eqn (19). Both figures therefore provide additional, although still qualitative, experimental evidence that the first kinetic hydriding regime is indeed likely to be limited by absorption and the second one by adsorption. It has to be recognised though that, although the p_{H_2} dependencies shown in Fig. 5 and 6 are consistent with our kinetic interpretation, the same graphs would still look more or less linear when claiming other reaction orders, like proportional with p_{H_2} for Fig. 5 or proportional to $1/(p_{H_2})^{1/2}$ for Fig. 6. Therefore, if one defines, respectively, S_{ab} and S_{ad} as the slopes and I_{ab} and I_{ad} as the intercepts of the claimed linear fits in Fig. 5 and 6, these parameters should as such also result in quantitatively relevant kinetic and thermodynamic hydriding parameters. This can be verified based on the following expressions:

$$\frac{S_{ad}}{Q} = \frac{2k'_{ad}K_{ab}^2}{(K_{ab}+n)^2 + K_{ab}} \tag{20}$$

$$\frac{I_{ad}}{Q} = \frac{-2k'_{ad}K_{ab}^2}{(K_{ab}+n)^2 + K_{ab}}(K_S n)^2 \tag{21}$$

$$\frac{S_{ab}}{Q} = -k'_{ab}K_S n \tag{22}$$

$$\frac{I_{ab}}{Q} = k'_{ab}(1-n) \tag{23}$$

Note that the proportionality constant Q has already been introduced before with eqn (3) in order to convert the measured velocities $(dn/dt)_{ad/ab}$ (expressed in s^{-1}) to the units of the data points in Fig. 5 and 6 (expressed in MPa s^{-1}).

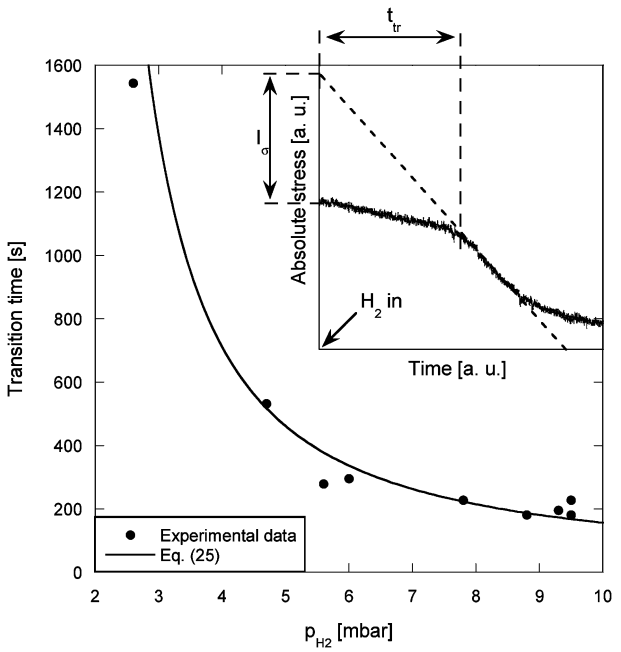

Fig. 7 Transition time between the first and second kinetic regimes as a function of p_{H_2}. A schematic construction indicating the definition of t_{tr} and I_σ in eqn (24) is included as well.

From eqn (20)–(23), it is clear that S_{ad} and I_{ab} should be positive, while S_{ab} and I_{ad} should be negative. This is indeed observed in the experimental fits obtained in Fig. 5 and 6. Before trying to solve the 4-equation system involving eqn (20)–(23), one can first define a time t_{tr} to indicate the transition between the first and second kinetic regime. As indicated in the inset of Fig. 7, this time should respect the following geometrical relationship:

$$\left[\left(\frac{dn}{dt}\right)_{ad}\Big|_{t=t_{tr}}\right]t_{tr} - \frac{I_\sigma}{Q} = \left[\left(\frac{dn}{dt}\right)_{ab}\Big|_{t=t_{tr}}\right]t_{tr} \tag{24}$$

where I_σ is the intercept of the linear fit through the second kinetic regime relative to the initial, as-deposited growth stress value (*cf.* the inset of Fig. 7). The latter parameter has been determined experimentally for all hydriding experiments, resulting in an average value of 446 ± 27 MPa, independent of p_{H_2} in the range 2–10 mbar considered here (*cf.* ESI†). By combining eqn (20)–(23) with eqn (24), we obtain

$$t_{tr} = \frac{I_\sigma}{\left(S_{ad}p_{H_2} - S_{ab}\frac{1}{\sqrt{p_{H_2}}} + I_{ad} - I_{ab}\right)} \tag{25}$$

Fig. 7 shows the experimental transition times, determined from the intersection of the linear fits in the first and second kinetic regimes, as well as their p_{H_2}-dependence predicted by eqn (25). For the latter, the S_i and I_i values were taken from the linear fits of Fig. 5 and 6. The excellent correlation obtained between the predicted and experimental t_{tr} values confirms that our kinetic model makes sense, both qualitatively and quantitatively.

The 4-equation system involving eqn (20)–(23) then provides a first access to some relevant kinetic and thermodynamic parameters, simply by dividing the slope and intercept values corresponding to the ad- and absorption limited regime:

$$\frac{S_{ad}}{I_{ad}} = -\frac{1}{(K_S n)^2} \tag{26}$$

$$\frac{S_{ab}}{I_{ab}} = -K_S\frac{n}{1-n} \tag{27}$$

Since we already determined the value of Sievert's constant K_s (*cf.* Fig. 4), eqn (26) gives a calculated average value for n of $(1.3 \pm 0.3) \times 10^{-2}$ for the second, adsorption-limited kinetic regime, while eqn (27) results in a calculated average n-value of $(1.4 \pm 0.4) \times 10^{-2}$ for the first, absorption-limited regime. These average values can indeed be considered to be sufficiently small in order for eqn (18) and (19) to result in the seemingly constant slopes observed in the first and second kinetic regimes. Moreover, its implication that n at $t = t_{tr}$ is independent of p_{H_2} is not surprising if one considers the constant compressive stress level of our samples at $t = t_{tr}$, which was found to be -94 ± 6 MPa relative to the initial, as-deposited growth stress value, independent of p_{H_2} (*cf.* ESI†).

As we now explicitly confirmed that $n \ll 1$ in this work, eqn (23) immediately results in $k'_{ab} = (7.4 \pm 0.8) \times 10^{-5}$ s^{-1} for the first regime. When taking $k''_{ab} = 1 \times 10^9$ s^{-1}, calculated at 298.15 K from ref. 33, and knowing that $K_{ab} \equiv k'_{ab}/k''_{ab}$, we obtain a value of $K_{ab} = (7.4 \pm 0.8) \times 10^{-14}$, and

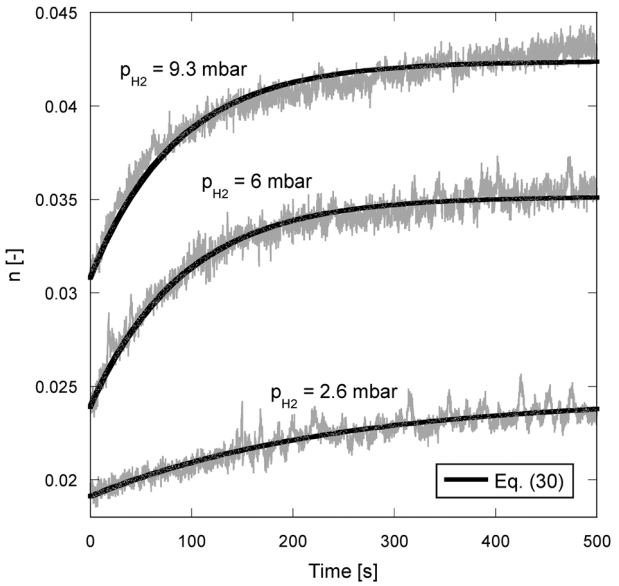

Fig. 8 Evolution of the bulk atomic concentration n in the third, non-linear kinetic regime for different values of p_{H_2}. The time scale has been shifted so that $t = 0$ s corresponds to the transition between the second and third kinetic regimes. The coarse solid lines correspond to a fit using eqn (30).

therefore $K_{ad} = (1.6 \pm 0.8) \times 10^{22}$ mbar^{-1} from eqn (10). The latter therefore also validates our earlier hypothesis of $p_{H_2}K_{ad} \gg 1$, needed for arriving at eqn (18). Moreover, inserting the calculated K_{ab} value and the previously obtained value of n into eqn (20) gives $k'_{ad} = (5 \pm 3) \times 10^{17}$ mbar^{-1} s^{-1}. As a value of K_{ad} has already been derived, and since $K_{ad} \equiv k'_{ad}/k''_{ad}$, one also arrives at $k''_{ad} = (3 \pm 2) \times 10^{-5}$ s^{-1}, in good agreement with the value of $k''_{ad} = 6.9 \times 10^{-5}$ s^{-1} calculated at 298.15 K from ref. 33.

Besides the presence of the two linear kinetic regimes analysed above, a third non-linear regime was resolved in Fig. 2 as well to precede the final hydriding equilibrium. Fig. 8 shows, for different p_{H_2}-values, the evolution of the bulk hydrogen concentration in this third kinetic regime, as calculated from the internal stress data using eqn (3). The time scale has been normalised to represent for each experiment the first 500 s of this regime. If we assume that absorption is the rate-limiting step in this regime, the temporal evolution of n can be deduced from eqn (18) by solving what is known as a basic Cauchy problem:[36]

$$\begin{cases} \dfrac{dn(t)}{dt} = n(t)C_1 + C_2 \\ n(t_0) = n_0 \end{cases} \qquad (28)$$

where t_0 refers to the transition time between the second and third kinetic regimes, and

$$\begin{cases} C_1 = -k'_{ab}\left(1 + \dfrac{K_S}{\sqrt{p_{H_2}}}\right) \\ C_2 = k'_{ab} \end{cases} \qquad (29)$$

The general solution of this problem is as follows:[36]

$$n(t) = \frac{-C_2}{C_1} + \left(n_0 + \frac{C_2}{C_1}\right)\exp(C_1(t - t_0)) \qquad (30)$$

The coarse solid lines in Fig. 8 correspond to the fits obtained with the absorption-related eqn (30). Intuitively, it can be understood that the third kinetic regime must indeed be limited by absorption because at the end of the second regime, the surface coverage has already reached its equilibrium value. In this case, the constant C_2 in eqn (29) then directly provides an estimate for k'_{ab}.

The thus obtained average value of C_2 for all experiments, calculated from fitting eqn (30) to the third kinetic regime, results in an average value of $k'_{ab} = (4.1 \pm 0.9) \times 10^{-4}$ s^{-1} for the third kinetic regime. Moreover, when repeating this procedure for the first kinetic regime, one gets $k'_{ab} = (3.3 \pm 0.8) \times 10^{-5}$ s^{-1}, consistent with the value of $k'_{ab} = (7.4 \pm 0.8) \times 10^{-5}$ s^{-1} previously obtained with the approximate eqn (23). The value of k'_{ab} for the first kinetic regime is however about one order of magnitude lower than the one characteristic for the third kinetic regime. Therefore, the major outcome of our kinetic study is that the absorption-controlled regimes I and III are characterised by very different values for k'_{ab}. In our opinion, this is related to the fact that the end of region I is being determined by a rather abrupt increase in the positive direction of the heat of adsorption. This is in line with ref. 31, where such an increase was reported to occur somewhere in the range $0.75 < \theta < 1$. In that case, k'_{ab} must increase as well since the potential energy surface for hydrogen adsorption/absorption indicates that the activation energy for hydrogen absorption should decrease if the heat of adsorption

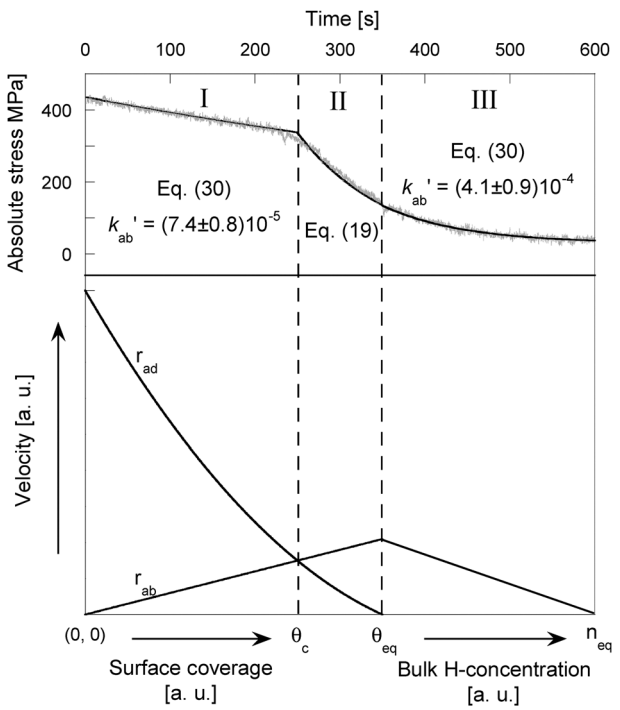

Fig. 9 Schematic representation of the θ-dependencies of the adsorption (r_{ad}) and absorption (r_{ab}) velocities, superimposed on the experimentally measured hydriding cycle at $p_{H_2} = 6$ mbar. Fits to the experimental data have been included as well, using constitutive eqn (30) for the absorption-controlled first and third regimes, and eqn (19) for the second, adsorption-limited regime. The values mentioned for k'_{ab} in regimes I and III represent average values derived from the fitting parameter C_2 (*cf.* eqn (29)) when including all experiments.

Table 1 Overview of the kinetic and thermodynamic hydriding parameters calculated in this work for Pd hydriding in the α phase region at 298 K, with the kinetic regimes which they apply to. Some values taken from the literature are displayed for comparison

Parameter	Origin	1st regime	2nd regime	3rd regime	Overall
k'_{ad}/mbar^{-1} s^{-1}	This work		$(5 \pm 3) \times 10^{17}$		
k''_{ad}/s^{-1}	This work		$(3 \pm 2) \times 10^{-5}$		
	Ref. 33				6.9×10^{-5}
K_{ad}/mbar^{-1}	This work				$(1.6 \pm 0.8) \times 10^{22}$
k'_{ab}/s^{-1}	This work	$(7.4 \pm 0.8) \times 10^{-5}$	$(4.1 \pm 0.9) \times 10^{-4}$	$(4.1 \pm 0.9) \times 10^{-4}$	
k''_{ab}/s^{-1}	Ref. 33				1×10^{9}
K_{ab}	This work				$(7.4 \pm 0.8) \times 10^{-14}$
K_s/atm$^{1/2}$	This work				3.3 ± 0.7
	Ref. 29				2

becomes less negative.[33] In this respect, we can also point out that the factor of 10 difference observed between k'_{ab} in regions 1 and 3 implies a coverage dependent change in activation energy on the order of $RT\ln(10)$, corresponding to 6 kJ mol^{-1} K^{-1} at 298 K. This number can indeed be considered to be a realistic change for a coverage dependant heat of adsorption, and is within the range of coverage dependence published for Pd surfaces.[31]

As a summary, Fig. 9 schematically represents the evolution of the adsorption and absorption velocities as a function of surface coverage, as can be anticipated from the current kinetic study. The velocities are superimposed on the experimentally measured hydriding cycle already shown in Fig. 2. The latter has also been simulated/fitted according to eqn (30) and (19). According to eqn (8), the θ-dependency of the adsorption velocity is a decreasing parabola, while, according to eqn (11), the absorption velocity increases linearly with θ. In the beginning of the experiment, the initial adsorption and absorption velocities are, respectively, $r_{ad} = k'_{ad}p_{H_2}$ and $r_{ab} = 0$. In the first linear kinetic regime, r_{ad} then rapidly decreases as θ reaches a value close to θ_{eq}. In this zone, eqn (11) predicts the rate-limiting absorption velocity dn/dt to increase linearly with θ and to decrease linearly with n, which is probably the reason why a constant average velocity is observed experimentally. When a critical value of the surface coverage is reached at the end of the first kinetic regime (denoted θ_c in Fig. 9), the heat of adsorption is believed to suddenly change in the positive direction. As a result, adsorption then becomes the new rate-limiting step, and the second kinetic regime starts. In this second zone, a plausible explanation for the observation of a constant average velocity is the fact that an increase in θ implies an increase in dn/dt. The increase of surface coverage is thus counterbalanced by the increasing absorption velocity, so that the apparent rate-limiting velocity appears as constant until adsorption equilibrium is reached. When the latter occurs at the end of the second stage ($\theta = \theta_{eq}$), the absorption velocity becomes rate-limiting again in the third kinetic regime. In this regime, dn/dt decreases with n and the kinetics are not linear anymore (*cf.* eqn (30)). An equilibrium stress plateau finally appears when absorption equilibrium is reached ($n = n_{eq}$).

Finally, Table 1 shows all the relevant kinetic and thermodynamic parameters calculated in this work, as well as the kinetic regimes to which they apply. Some literature values are also included, like the constant k''_{ab} that we used in this study for some of the related calculations. Other reference values from the literature show the overall consistency of the obtained results.

4. Conclusions

A new *in situ* diagnostic tool, based on the real-time monitoring of hydriding-induced internal stresses, has been used for the *in situ* study of the hydriding kinetics of Pd thin films. Three different kinetic regimes have been resolved. The first two exhibited a linear increase of the internal stress in the compressive direction with time. A systematic study of the p_{H_2}-dependency of these two constant slopes, based on newly derived constitutive equations, resulted in the identification of the first linear regime to be limited by absorption and the second one by adsorption. After adsorption equilibrium is reached at the end of the second stage, a third, non-linear kinetic regime, limited by absorption, was found to precede the final equilibrium. The quantitative analysis of these different regimes resulted in the calculation of a number of relevant kinetic and thermodynamic hydriding parameters. One of the major outcomes in this respect is that the rate constant for hydrogen absorption k'_{ab} in the first and third kinetic regimes differs by almost one order of magnitude. This has been attributed to the fact that the end of the first regime is being determined by a rather abrupt increase in the positive direction of the heat of adsorption. As a result, this study was able to provide a self-consistent quantitative interpretation of the entire room temperature Pd hydriding cycle in the α-phase domain.

Acknowledgements

We gratefully acknowledge Marc Sinnaeve for technical support with the development of the experimental setup, and Prof. Juray De Wilde and Philippe Eliaers for insightful discussions on the constitutive kinetic equations. We are particularly grateful to one of the reviewers for his suggestions in constructing the kinetic model. This work was funded by the Belgian National Science Foundation through a FRIA doctoral fellowship.

References

1 E. Wicke and H. Brodowsky, in *Hydrogen in metals*, ed. G. Alefeld and J. Voelkl, Springer, Berlin, Germany, 1978, vol. 2, pp. 73-155.
2 F. A. Lewis, *The palladium hydrogen system*, Academic Press, London, UK, 1967.
3 E. L. Fleischer, *MRS Bull.*, 2002, **27**(9), 675–716.

4 P. Chen and M. Zhu, *Mater. Today*, 2008, **11**, 36–43.
5 R.-H. Jones and G. Thomas, *JOM*, 2007, **59**, 50–55.
6 Z. Zhao, Y. Sevryugina, M. A. Carpenter, D. Welch and H. Xia, *Anal. Chem.*, 2004, **76**, 6321–6326.
7 A. Kulprathipanja, G. O. Alptekin, J. L. Falconer and J. D. Way, *J. Membr. Sci.*, 2005, **254**, 49–62.
8 L. L. Jewell and B. H. Davis, *Appl. Catal., A*, 2006, **310**, 1–15.
9 Z. Hu, T. Thundat and R. J. Warmack, *J. Appl. Phys.*, 2001, **90**, 427–431.
10 W. Vogel, W. He, Q.-H. Huang, Z. Zou, X.-G. Zhang and H. Yang, *Int. J. Hydrogen Energy*, 2010, **35**, 8609–8620.
11 M. Suleiman, N. M. Jisrawi, O. Dankert, M. T. Reetz, C. Bähtz, R. Kircheim and A. Pundt, *J. Alloys Compd.*, 2003, **356–357**, 644–648.
12 A. Pundt and R. Kircheim, *Annu. Rev. Mater. Res.*, 2006, **36**, 555–608.
13 R. J. Matelon, J. I. Avila, U. G. Volkmann, A. L. Cabrera, E. H. Morales and D. Lederman, *Thin Solid Films*, 2008, **516**, 7797–7801.
14 T. P. Leervad Pedersen, C. Liesch, C. Salinga, T. Eleftheriadis, H. Weis and M. Wuttig, *Thin Solid Films*, 2004, **458**, 299–303.
15 C. Lemier and J. Weissmüller, *Acta Mater.*, 2007, **55**, 1241–1254.
16 M. Pasturel, M. Slaman, H. Schreuders, J. H. Rector, D. M. Borsa, B. Dam and R. Griessen, *J. Appl. Phys.*, 2006, **100**, 023515.
17 R. Delmelle, G. Bamba and J. Proost, *Int. J. Hydrogen Energy*, 2010, **35**, 9888–9892.
18 Q. Van Overmeere, J.-F. Vanhumbeeck and J. Proost, *Rev. Sci. Instrum.*, 2010, **81**, 045106.
19 J. Proost and F. Spaepen, *J. Appl. Phys.*, 2002, **91**, 204–216.
20 N. Joshi, D. K. Aswal, A. K. Debnath, S. K. Gupta and J. V. Yakhmi, *Appl. Surf. Sci.*, 2004, **228**, 302–305.
21 U. Singh, N. Jha, T. P. Singh, A. Kapoor and A. Perrone, *Opt. Laser Technol.*, 2010, **42**, 1128–1133.
22 S. Bouhtiyya and L. Roué, *Int. J. Hydrogen Energy*, 2008, **33**, 2912–2920.
23 A. Kern and W. Eysel, *Mineralogisch-Petrograph. Inst.*, Univ. Heidelberg, Germany, ICDD Grant-in-Aid, 1993.
24 M. M. El Gowini and W. A. Moussa, *Sensors*, 2010, **10**, 1232–1250.
25 H. Peisl, *Hydrogen in metals*, ed. G. Alefeld and J. Voelkl, Springer, Berlin, Germany, 1978, vol. 1, pp. 57–73.
26 A. Pundt, E. Nikitin, P. Pekarski and R. Kirchheim, *Acta Mater.*, 2004, **52**, 1579–1587.
27 P. G. Sanders, J. A. Eastman and J. R. Weertman, *Acta Mater.*, 1997, **45**, 4019–4025.
28 C. J. Smithells, *Metals reference book*, Butterworths, London, UK, 2004, p. 1258.
29 R. V. Bucur, *J. Mater. Sci.*, 1987, **22**, 3402–3406.
30 R. V. Bucur, *Surf. Sci.*, 1977, **62**, 519–535.
31 M. Johansson, E. Skúlason, G. Nielsen, S. Murphy, R. M. Nielsen and I. Chorkendorff, *Surf. Sci.*, 2010, **604**, 718–729.
32 S. Hong and T. S. Rahman, *Phys. Rev. B: Condens. Matter Mater. Phys.*, 2007, **75**, 155405.
33 T. L. Ward and T. Dao, *J. Membr. Sci.*, 1999, **153**, 211–231.
34 J. B. Rawlings and J. G. Ekerdt, *Chemical reactor analysis and design fundamentals*, Nob Hill Pub., Madison, USA, 2002, pp. 189–277.
35 G. G. Froment, K. B. Bischoff and J. De Wilde, *Chemical reactor analysis and design*, John Wiley & Sons, 2010, 3rd edn, pp. 60–81.
36 A. D. Polyanin and V. F. Zaitsev, *Handbook of exact solutions for ordinary differential equations*, Chapman & Hall/CRC Press, Boca Raton, USA, 2003.